NANO LETTERS

Letter

pubs.acs.org/NanoLett

Ambipolar Field Effect in Sb-Doped Bi_2Se_3 Nanoplates by Solvothermal Synthesis

Desheng Kong,[†,∥] Kristie J. Koski,[†,∥] Judy J. Cha,[†] Seung Sae Hong,[‡] and Yi Cui*[,†,§]

[†]Department of Materials Science & Engineering, Stanford University, Stanford, California 94305, United States

[‡]Department of Applied Physics, Stanford University, Stanford, California 94305, United States

[§]Stanford Institute for Materials and Energy Sciences, SLAC National Accelerator Laboratory, 2575 Sand Hill Road, Menlo Park, California 94025, United States

Supporting Information

ABSTRACT: A topological insulator is a new phase of quantum matter with a bulk band gap and spin-polarized surface states, which might find use in applications ranging from electronics to energy conversion. Despite much exciting progress in the field, high-yield solution synthesis has not been widely used for the study of topological insulator behavior. Here, we demonstrate that solvothermally synthesized Bi_2Se_3 nanoplates are attractive for topological insulator studies. The carrier concentration of these Bi_2Se_3 nanoplates is controlled by compensational Sb doping during the synthesis. In low-carrier-density, Sb-doped Bi_2Se_3 nanoplates, we observe pronounced ambipolar field effect that demonstrates the flexible manipulation of carrier type and concentration for these nanostructures. Solvothermal synthesis offers an affordable, facile approach to produce high-quality nanomaterials to explore the properties of topological insulators.

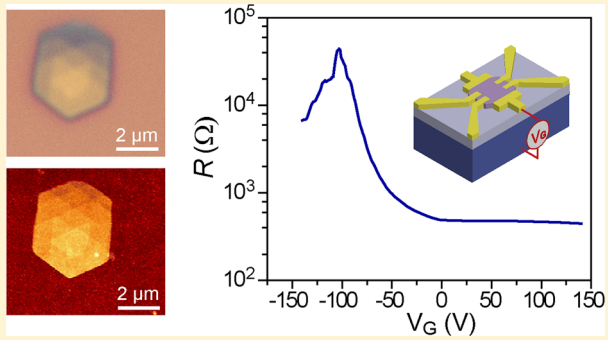

KEYWORDS: *Topological insulator, solvothermal synthesis, Bi_2Se_3 nanoplate, ambipolar field effect, Sb doping, low carrier density*

Topological insulators represent a novel class of semiconductors with spin-polarized metallic surface states[1−5] which exhibit inherent robustness and unique electronic properties with potential applications in low-energy dissipation electronics,[6] thermoelectrics,[4,7,8] catalysis,[9] and near-infrared transparent electrodes.[10] In most proposed applications, suppressing excessive bulk carriers is required, which might otherwise mask the effect of topological surface carriers. These residual bulk carriers usually come from crystal defects[11] or environmental doping.[12−14] To meet the stringent requirements for these applications, controlling bulk carriers of topological insulators is broadly explored by means of chemical doping,[12,13,15−17] electrostatic gating,[18−25] and nanostructuring with increased surface-to-volume ratios,[26] based on high-temperature-grown bulk single crystals,[12,13,15−17] vapor-phase-grown nanocrystals,[24,26−29] mechanically exfoliated flakes,[19,30] and molecular beam epitaxy films.[31−33]

Wet, chemically synthesized nanocrystals are rarely explored in the context of topological insulators despite the fact that the majority of topological insulators are also room temperature thermoelectric materials, such as Bi_xSb_{1-x}, Bi_2Se_3, Bi_2Te_3, Sb_2Te_3, $(Bi_xSb_{1-x})_2Te_3$, $Bi_2(Se_xTe_{1-x})_3$, Heusler, and Half-Heusler compounds,[15,22,33−42] due to coincidentally similar criteria of candidate materials.[4] Previously, diverse methods of solution synthesis have been demonstrated as attractive avenues to mass-produce high-performance thermoelectric materials.[43,44] Recently, high mobility surface carriers were observed on solvothermally synthesized topological insulator nanoribbons of Bi_2Te_3,[45] demonstrating the promise of solution growth for topological insulator studies. Despite the encouraging progress, an effective approach to suppress bulk carriers in these solution-synthesized nanocrystals has not been achieved, limiting their potential in topological insulator studies. Here, we use a solvothermal reaction to grow Sb-doped nanoplates of Bi_2Se_3. Systematic transport measurements confirm that Sb-doping effectively reduces the bulk carrier density. We observe a clear ambipolar field effect in Sb-doped nanoplates with low carrier density, as expected for a topological insulator transistor device. Solvothermally synthesized topological insulator nanostructures exhibit exceptional crystalline quality to investigate the physical properties of these novel materials.

Bi_2Se_3 is a layered chalcogenide with a rhombohedral crystal structure of space group D^5_{3d} (R-3m) as shown in Figure 1A. Each layer consists of five shifted selenium and bismuth atomic planes stacked along c-axis in the sequence of Se(1)−Bi−Se(2)−Bi−Se(1), termed a quintuple layer (∼1 nm in thickness). Here, nanoplates of Bi_2Se_3 are synthesized using a solvothermal reaction. Polyvinylpyrrolidone (0.5 g, Sigma-Aldrich), ethylenediaminetetraacetic acid (EDTA, 1 g, Sigma-

Received: November 14, 2012
Revised: January 9, 2013

   dx.doi.org/10.1021/nl304212u | *Nano Lett.* XXXX, XXX, XXX−XXX

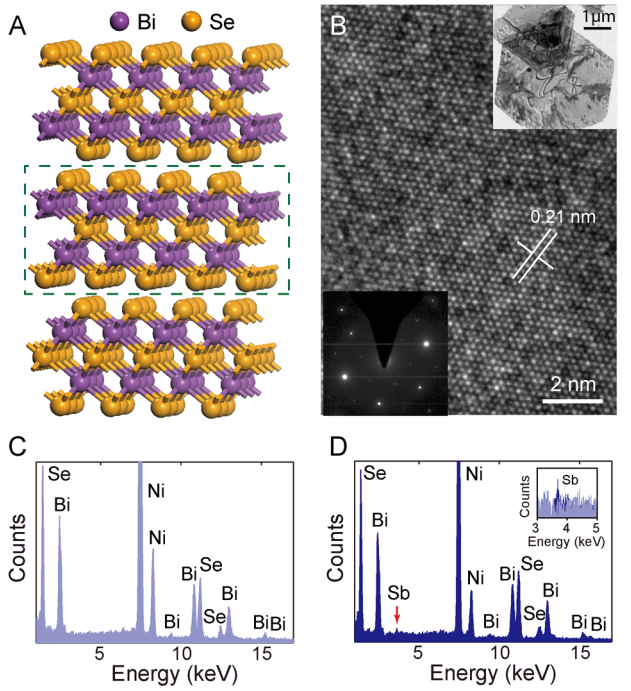

Figure 1. (A) Layered rhombohedral crystal structure of Bi_2Se_3. Dashed green line indicates a Se(1)−Bi−Se(2)−Bi−Se(1) quintuple layer with thicknesss of ∼1 nm. (B) TEM characterization of solvothermally synthesized Bi_2Se_3 nanoplates on a nickel-grid-supported lacey carbon film. The high-resolution TEM image is taken along the [0001] direction, clearly revealing crystalline lattice fringes. The corresponding nanoplate is shown in the top-right inset. Sharp diffraction spots in the selected area diffraction pattern (bottom-left inset) further confirm the nanoplate is a high-quality crystal. (C) EDS spectrum of a pure Bi_2Se_3 nanoplate. (D) EDS spectrum of an Sb-doped Bi_2Se_3 nanoplate. Inset: stacked EDS spectra of the pure and Sb-doped nanoplates, showing the presence of Sb in the doped sample. The Sb peak in Sb-doped Bi_2Se_3 roughly corresponds to an atomic percentage of 1%.

Aldrich), bismuth oxide (Bi_2O_3, 0.47 g, Sigma-Aldrich), and an excess of selenium powder (0.29 g, Aldrich) are added into 40 mL of ethylene glycol (from EMD) and stirred vigorously for 2 h. The average lateral size of the nanoplates can be controlled by adjusting the concentration of EDTA. The solution is transferred into a Teflon-lined stainless steel autoclave and heated at 165 °C for 8−12 h. Previous studies suggest Sb serves as compensational dopant that suppresses bulk electron density in Bi_2Se_3. To dope Bi_2Se_3 nanoplates with a nominal amount of Sb during synthesis, the same synthetic procedure is carried out yet antimony acetate (0.30 g, Alfa Aesar) is added to the initial solution along with a reduced amount of Bi_2O_3 (0.23 g). Antimony acetate, on heating, decomposes to give antimony oxide (Sb_2O_3), which is the active antimony source in these experiments. Antimony oxide powder can also be used as a doping precursor. The use of an acetate salt increases the average lateral size of the nanoplates as seen in other studies.[46] Nanoplates are cleaned by centrifugation at 1460 rpm for 10 min three times, redispersed, and stored in 99% ethanol (Alfa Aesar). Nanoplates used in these studies are stored under ambient conditions for upward of 1−4 weeks before device fabrication and physical property measurements. No obvious degradation of sample quality or transport properties has been observed. PVP coating may help prevent sample degradation from environmental factors.[45]

Synthesized nanoplates are characterized by transmission electron microcopy (TEM, FEI Tecnai F20 microscope operated at 200 kV). TEM samples are prepared by drop-casting the suspension onto lacey carbon films supported by Ni grids. Nanoplates lie flat on the membrane from the surface tension generated by evaporation of the ethanol. TEM analysis on nanoplates of pure and Sb-doped Bi_2Se_3 are summarized in Figure S1 and Figure 1B, respectively. As-grown nanoplates typically exhibit hexagonal morphology with 120° edge facets and lateral dimension in micrometers but typically less than 20 μm. The sharp diffraction pattern in selected area electron diffraction and clear lattice fringes in high-resolution TEM images (HRTEM) confirm the single-crystalline nature of these nanoplates. The lattice spacing in HRTEM is ∼0.21 nm, well matching the expected spacing of (11-20) planes. The compositions of individual nanoplates are determined by energy dispersive X-ray spectroscopy (EDS). An EDS spectrum from pure Bi_2Se_3 shows stoichiometry of Bi/Se ∼ 2/3, whereas the EDS spectrum from Sb-doped samples (Figure 1D) reveals identifiable Sb peak corresponding to an atomic percentage of ∼1%, which confirms that Sb is successfully incorporated into the nanoplates during the solvothermal reaction. Sb_2Se_3 naturally crystallizes in orthorhombic structure, whereas Bi_2Se_3 stabilizes in layered rhombohedral structure. Accordingly, Sb exhibits limited solubility in ternary rhombohedral $(Bi_xSb_{1-x})_2Se_3$, in sharp constrast to the ternary $(Bi_xSb_{1-x})_2Te_3$ system that crystallizes in rhombohedral for the entire composition range.[22] We notice that the Sb percentage in solvothermally synthesized nanoplate is much lower than that of vapor-phase-synthesized nanoribbon (up to 7 at. %),[24] likely due to the lower reaction temperature.

Bi_2Se_3 nanoplates can easily be identified in optical microscopy images. Certain substrates, such as the oxidized silicon with 300 nm thick SiO_2 layer used here, dramatically enhance the optical contrast to manifest thickness differences down to a single quintuple layer.[28] Figure 2A is a typical optical

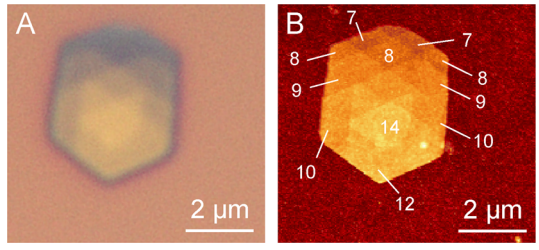

Figure 2. (A) An optical image of an Sb-doped Bi_2Se_3 nanoplate on an oxidized silicon substrate (300 nm SiO_2/Si) showing thickness-dependent optical contrast. (B) Corresponding AFM image of the same nanoplate. The number of quintuple layers is marked in the image. This nanoplate has multiple quintuple layer steps suggesting a layer-by-layer growth solution process.

image of an Sb-doped Bi_2Se_3 nanoplate on an oxidized silicon substrate, acquired by an Olympus BX51M microscope under normal white-light illumination. The optical contrast distribution suggests the presence of multiple steps with 60° or 120° facets. This is further confirmed with correlated atomic force microscopy (AFM, Park System XE-70) measurements (Figure 2B), revealing steps with thicknesses ranging from 6 to 14 quintuple layers. The presence of multiple steps on individual nanoplates suggests a layer-by-layer growth process during the solvothermal reaction. This is likely due to the anisotropic

dx.doi.org/10.1021/nl304212u | Nano Lett. XXXX, XXX, XXX−XXX

crystal structure with high-energy edges and dangling bonds predominately distributed on the side surfaces that readily bind additional adatoms in planar growth. We note that AFM measurements are affected by residual PVP surfactant on the surface of the nanoplate. To unambiguously determine the actual thickness, we use Ar plasma etched, vapor-phase-synthesized Bi_2Se_3 nanoribbons establishing a correlation between optical contrast and sample thickness (Figure S2). Accordingly, optical imaging provides a facile gauge of the sample thickness. The thickness of residual surfactant coating on solvothermally synthesized nanoplates ranges from a few angstroms to ~3 nm (Figures S3 and S4).

Electrical properties of solvothermally grown Bi_2Se_3 nanoplates are studied in single nanoplate devices. As-grown nanoplates are drop-cast on oxidized silicon substrates with a prepatterned metal marker array. Nanoplates free of terraces are selected according to their optical contrast for transport studies to simplify data interpretation. We notice these nanoplates are mainly in the thinner range of the thickness distribution, suggesting additional terraces tend to nucleate and grow as the nanoplates get thicker. Electrodes are fabricated onto each nanoplate by standard e-beam lithography and thermal evaporation of Cr/Au films (10 nm/100 nm) with the six-terminal Hall bar geometry (schematic shown as the inset of Figure 3A). To ensure reliable ohmic contacts, a gentle Ar plasma etching process is performed in a sputtering chamber to remove residual PVP and EDTA on the nanoplates right before metal film deposition. All the transport measurements are carried out at 2 K inside an Oxford cryostat with a digital lock-in amplifier (Stanford Research Systems SR830), and the thickness of individual nanoplate is determined by the optical contrast and the AFM measurements (Supporting Information). The area carrier density and mobility values obtained from Hall measurements are summarized in Figures 3A and 3B, respectively. To compare the results with other synthetic approaches, we adopt the empirical curves of carrier density and mobility from Kim et al.,[47] shown as the green curves in Figure 3, obtained from their MBE films and bulk single crystals of pure Bi_2Se_3.[13] Apparently, pure Bi_2Se_3 from solvothermal growth exhibits higher carrier density than the empirical values, presumably due to the low reaction temperature which favors the formation of Se vacancies. High-quality MBE films are typically grown at 190−250 °C[31] and bulk crystals at 550−750 °C.[13] The mobility values of pure Bi_2Se_3 nanoplates are also lower than MBE films. Sb doping effectively reduces the carrier density and enhances the mobility approaching the properties of MBE films, indicating significant improvement of the crystal quality. Notice that all the nanoplates measured here are thicker than the critical thickness of ~6 nm for Bi_2Se_3, below which the surface states between the top and bottom surfaces of the nanoplate may hybridize to form a conventional semiconductor or 2D quantum spin Hall system.[31,48,49] The effective carrier concentrations and Hall mobility values presented here have the contributions from both the bulk and surface carriers. The lack of distinctive signatures in magnetotransport prevents us from analyzing each components in a quantitative manner, so we limit our discussion to the effective carrier concentration and mobility.

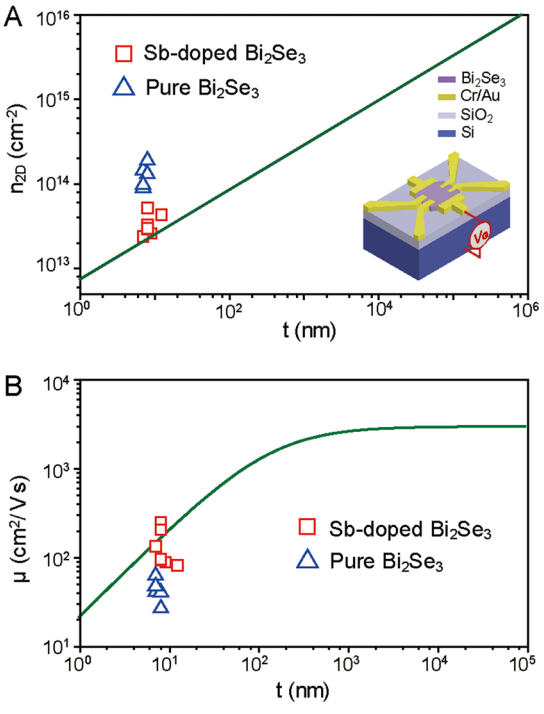

Figure 3. Comparison of solvothermally synthesized Bi_2Se_3 nanoplates with other synthetic approaches. (A) Summary of area carrier density n_{2D} of pure Bi_2Se_3 and Sb-doped Bi_2Se_3 nanoplates. In comparison, the green trace is the empirical relation of n_{2D} versus the sample thickness t from MBE films and bulk single crystals by Kim et al.[47] Inset: schematic diagram of the device structure. (B) Summary of electron mobility, μ, of pure Bi_2Se_3 and Sb-doped Bi_2Se_3 nanoplates, in comparison with the MBE films and bulk single crystals (green trace).

The properties of Sb-doped nanoplates are further explored with backgate field effect transistor devices. Solvothermally synthesized nanoplates suspended and stored in ethanol are readily transferred onto various substrates by drop-casting. Here, we use a 300 nm thick SiO_2 dielectric layer on a degenerately doped n-type silicon substrate to apply a backgate voltage (device schematic shown as the inset of Figure 3A). The spread of carrier density of Sb-doped samples falls into an interesting range, allowing us to access distinctive gating behaviors. In Sb-doped nanoplates with low carrier density, we have observed a pronounced field effect (Figure 4A). Typical dependence of the resistance on the gate voltage, V_G, exhibits a sharp peak that is 2 orders of magnitude higher than the resistance at large V_G. The Hall coefficient, R_H, also reverses its sign near the peak of the resistance, changing from the original n-type conductor to a p-type conductor through a mixed state with the coexistence of electrons and holes. Such an ambipolar field effect requires the effective suppression of bulk carriers, a characteristic behavior for low-density topological insulator nanoplates,[22−24] which is also previously observed in graphene—another material with gapless two-dimensional Dirac fermions.[50] In nanoplates with moderate carrier density (Figure 4B), a strong field effect is still observed, where R and $|R_H|$ increase a few times by applying large negative voltage. Although the nanoplate cannot be fully inverted into p-type within the limit of gate voltage, the clear response by electrostatic gating corresponds to effective carrier depletion. In nanoplates with high carrier density, however, the changes of R and $|R_H|$ by applying a backgate voltage are much smaller, suggesting the dominance of excessive bulk carriers in the charge transport process irrespective of the external electric field. Apparently, the initial carrier density largely determines the behaviors of electrostatic gating for Bi_2Se_3 nanoplates, and

dx.doi.org/10.1021/nl304212u | Nano Lett. XXXX, XXX, XXX−XXX

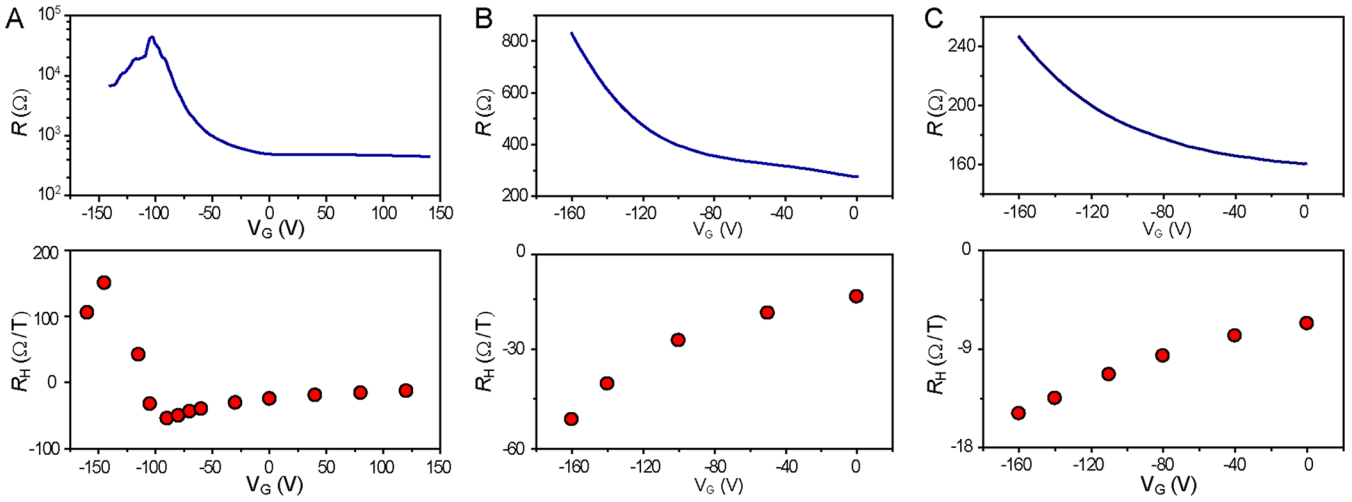

Figure 4. Field effect of Sb-doped Bi_2Se_3 nanoplates. (A) Pronounced ambipolar field effect observed on a typical nanoplate with low carrier density ($n_{2D} \sim 2.6 \times 10^{13}$ cm^{-2} at $V_G = 0$). The resistance, R, exhibits a sharp peak by changing the backgate voltage, V_G (top row). The corresponding Hall coefficient R_H (bottom row) exhibits a sign reversal at the V_G of the peak in R. (B) Field effect on a nanoplate with moderate carrier density ($n_{2D} \sim 4.3 \times 10^{13}$ cm^{-2} at $V_G = 0$). R shows a monotonic increase of several times, at the large negative bias voltage. R_H exhibits a consistent monotonic change with V_G. (C) Field effect on a nanoplate with high carrier density ($n_{2D} \sim 9.4 \times 10^{13}$ cm^{-2} at $V_G = 0$). R shows a monotonic increase, but with very small magnitude at the large negative bias voltage. R_H also shows weak response with bias voltage.

compensational Sb doping is therefore critical to enhance the electrical field effect by reducing the intrinsic carrier density.

This work provides a systematic study of Sb-doped Bi_2Se_3 nanoplates synthesized by a solvothermal reaction in the context of topological insulators. Sb doping allows access of nanoplates with low carrier density, which can be further suppressed by electrostatic gating. A pronounced ambipolar field effect is observed in certain Sb-doped nanoplate transistor devices, demonstrating the flexible manipulation of carrier type and density in these nanostructures. Solution derived nanocrystals afford an alternative approach to access high-quality topological insulator materials.

■ ASSOCIATED CONTENT

Ⓢ Supporting Information

Additional TEM characterization, optical images, AFM measurements, and volume carrier density versus nanoplate thickness. This material is available free of charge via the Internet at http://pubs.acs.org.

■ AUTHOR INFORMATION

Corresponding Author

*E-mail yicui@stanford.edu.

Author Contributions

The manuscript was written through contributions of all authors. All authors have given approval to the final version of the manuscript.

Author Contributions

‖These authors contributed equally.

Notes

The authors declare no competing financial interest.

■ ACKNOWLEDGMENTS

Y.C. acknowledges support from the Keck Foundation and DARPA MESO project (no. N66001-11-1-4105). Y.C. also acknowledges support from the Department of Energy, Office of Basic Energy Sciences, Materials Sciences and Engineering Division, under contract DE-AC02-76-SFO0515.

■ REFERENCES

(1) Hasan, M. Z.; Kane, C. L. *Rev. Mod. Phys.* **2010**, *82* (4), 3045.
(2) Qi, X.-L.; Zhang, S.-C. *Rev. Mod. Phys.* **2011**, *83* (4), 1057−1110.
(3) Moore, J. E. *Nature* **2010**, *464* (7286), 194−198.
(4) Kong, D.; Cui, Y. *Nat. Chem.* **2011**, *3* (11), 845−849.
(5) Müchler, L.; Zhang, H.; Chadov, S.; Yan, B.; Casper, F.; Kübler, J.; Zhang, S.-C.; Felser, C. *Angew. Chem., Int. Ed.* **2012**, *51* (29), 7221−7225.
(6) Qi, X.-L.; Zhang, S.-C. *Phys. Today* **2010**, *63* (1), 33−38.
(7) Ghaemi, P.; Mong, R. S. K.; Moore, J. E. *Phys. Rev. Lett.* **2010**, *105* (16), 166603.
(8) Tretiakov, O. A.; Abanov, A.; Murakami, S.; Sinova, J. *Appl. Phys. Lett.* **2010**, *97* (7), 073108−3.
(9) Chen, H.; Zhu, W.; Xiao, D.; Zhang, Z. *Phys. Rev. Lett.* **2011**, *107* (5), 056804.
(10) Peng, H.; Dang, W.; Cao, J.; Chen, Y.; Wu, D.; Zheng, W.; Li, H.; Shen, Z.-X.; Liu, Z. *Nat. Chem.* **2012**, *4* (4), 281−286.
(11) Wang, G.; Zhu, X.-G.; Sun, Y.-Y.; Li, Y.-Y.; Zhang, T.; Wen, J.; Chen, X.; He, K.; Wang, L.-L.; Ma, X.-C.; Jia, J.-F.; Zhang, S. B.; Xue, Q.-K. *Adv. Mater.* **2011**, *23* (26), 2929−2932.
(12) Analytis, J. G.; McDonald, R. D.; Riggs, S. C.; Chu, J.-H.; Boebinger, G. S.; Fisher, I. R. *Nat. Phys.* **2010**, *6* (12), 960−964.
(13) Analytis, J. G.; Chu, J.-H.; Chen, Y.; Corredor, F.; McDonald, R. D.; Shen, Z. X.; Fisher, I. R. *Phys. Rev. B* **2010**, *81* (20), 205407.
(14) Kong, D.; Cha, J. J.; Lai, K.; Peng, H.; Analytis, J. G.; Meister, S.; Chen, Y.; Zhang, H.-J.; Fisher, I. R.; Shen, Z.-X.; Cui, Y. *ACS Nano* **2011**, *5* (6), 4698−4703.
(15) Chen, Y. L.; Analytis, J. G.; Chu, J.-H.; Liu, Z. K.; Mo, S.-K.; Qi, X. L.; Zhang, H. J.; Lu, D. H.; Dai, X.; Fang, Z.; Zhang, S. C.; Fisher, I. R.; Hussain, Z.; Shen, Z.-X. *Science* **2009**, *325* (5937), 178−181.
(16) Hor, Y. S.; Richardella, A.; Roushan, P.; Xia, Y.; Checkelsky, J. G.; Yazdani, A.; Hasan, M. Z.; Ong, N. P.; Cava, R. J. *Phys. Rev. B* **2009**, *79* (19), 195208.
(17) Chen, Y. L.; Chu, J.-H.; Analytis, J. G.; Liu, Z. K.; Igarashi, K.; Kuo, H.-H.; Qi, X. L.; Mo, S. K.; Moore, R. G.; Lu, D. H.; Hashimoto, M.; Sasagawa, T.; Zhang, S. C.; Fisher, I. R.; Hussain, Z.; Shen, Z. X. *Science* **2010**, *329* (5992), 659−662.
(18) Chen, J.; Qin, H. J.; Yang, F.; Liu, J.; Guan, T.; Qu, F. M.; Zhang, G. H.; Shi, J. R.; Xie, X. C.; Yang, C. L.; Wu, K. H.; Li, Y. Q.; Lu, L. *Phys. Rev. Lett.* **2010**, *105* (17), 176602.
(19) Checkelsky, J. G.; Hor, Y. S.; Cava, R. J.; Ong, N. P. *Phys. Rev. Lett.* **2011**, *106* (19), 196801.

(20) Chen, J.; He, X. Y.; Wu, K. H.; Ji, Z. Q.; Lu, L.; Shi, J. R.; Smet, J. H.; Li, Y. Q. *Phys. Rev. B* **2011**, *83* (24), 241304.
(21) Steinberg, H.; Gardner, D. R.; Lee, Y. S.; Jarillo-Herrero, P. *Nano Lett.* **2010**, *10* (12), 5032−5036.
(22) Kong, D.; Chen, Y.; Cha, J. J.; Zhang, Q.; Analytis, J. G.; Lai, K.; Liu, Z.; Hong, S. S.; Koski, K. J.; Mo, S.-K.; Hussain, Z.; Fisher, I. R.; Shen, Z.-X.; Cui, Y. *Nat. Nanotechnol.* **2011**, *6* (11), 705−709.
(23) Kim, D.; Cho, S.; Butch, N. P.; Syers, P.; Kirshenbaum, K.; Adam, S.; Paglione, J.; Fuhrer, M. S. *Nat. Phys.* **2012**, in press.
(24) Hong, S. S.; Cha, J. J.; Kong, D.; Cui, Y. *Nat. Commun.* **2012**, *3*, 757.
(25) Yuan, H.; Liu, H.; Shimotani, H.; Guo, H.; Chen, M.; Xue, Q.; Iwasa, Y. *Nano Lett.* **2011**, *11* (7), 2601−2605.
(26) Peng, H.; Lai, K.; Kong, D.; Meister, S.; Chen, Y.; Qi, X.-L.; Zhang, S.-C.; Shen, Z.-X.; Cui, Y. *Nat. Mater.* **2010**, *9* (3), 225−229.
(27) Kong, D.; Randel, J. C.; Peng, H.; Cha, J. J.; Meister, S.; Lai, K.; Chen, Y.; Shen, Z.-X.; Manoharan, H. C.; Cui, Y. *Nano Lett.* **2010**, *10* (1), 329−333.
(28) Kong, D.; Dang, W.; Cha, J. J.; Li, H.; Meister, S.; Peng, H.; Liu, Z.; Cui, Y. *Nano Lett.* **2010**, *10* (6), 2245−2250.
(29) Cha, J. J.; Kong, D.; Hong, S.-S.; Analytis, J. G.; Lai, K.; Cui, Y. *Nano Lett.* **2012**, *12* (2), 1107−1111.
(30) Teweldebrhan, D.; Goyal, V.; Balandin, A. A. *Nano Lett.* **2010**, *10* (4), 1209−1218.
(31) Zhang, Y.; He, K.; Chang, C.-Z.; Song, C.-L.; Wang, L.-L.; Chen, X.; Jia, J.-F.; Fang, Z.; Dai, X.; Shan, W.-Y.; Shen, S.-Q.; Niu, Q.; Qi, X.-L.; Zhang, S.-C.; Ma, X.-C.; Xue, Q.-K. *Nat. Phys.* **2010**, *6* (8), 584−588.
(32) Li, Y. Y.; Wang, G.; Zhu, X. G.; Liu, M. H.; Ye, C.; Chen, X.; Wang, Y. Y.; He, K.; Wang, L. L.; Ma, X. C.; Zhang, H. J.; Dai, X.; Fang, Z.; Xie, X. C.; Liu, Y.; Qi, X. L.; Jia, J. F.; Zhang, S. C.; Xue, Q. K. *Adv. Mater.* **2010**, *22* (36), 4002−4007.
(33) Zhang, J.; Chang, C.-Z.; Zhang, Z.; Wen, J.; Feng, X.; Li, K.; Liu, M.; He, K.; Wang, L.; Chen, X.; Xue, Q.-K.; Ma, X.; Wang, Y. *Nat. Commun.* **2011**, *2*, 574.
(34) Fu, L.; Kane, C. L. *Phys. Rev. B* **2007**, *76* (4), 045302.
(35) Hsieh, D.; Qian, D.; Wray, L.; Xia, Y.; Hor, Y. S.; Cava, R. J.; Hasan, M. Z. *Nature* **2008**, *452* (7190), 970−974.
(36) Zhang, H.; Liu, C.-X.; Qi, X.-L.; Dai, X.; Fang, Z.; Zhang, S.-C. *Nat. Phys.* **2009**, *5* (6), 438−442.
(37) Xia, Y.; Qian, D.; Hsieh, D.; Wray, L.; Pal, A.; Lin, H.; Bansil, A.; Grauer, D.; Hor, Y. S.; Cava, R. J.; Hasan, M. Z. *Nat. Phys.* **2009**, *5* (6), 398−402.
(38) Wang, L.-L.; Johnson, D. D. *Phys. Rev. B* **2011**, *83* (24), 241309.
(39) Ren, Z.; Taskin, A. A.; Sasaki, S.; Segawa, K.; Ando, Y. *Phys. Rev. B* **2010**, *82* (24), 241306.
(40) Xiong, J.; Petersen, A. C.; Qu, D.; Hor, Y. S.; Cava, R. J.; Ong, N. P. *Phys. E (Amsterdam, Neth.)* **2012**, *44* (5), 917−920.
(41) Chadov, S.; Qi, X.; Kübler, J.; Fecher, G. H.; Felser, C.; Zhang, S. C. *Nat. Mater.* **2010**, *9* (7), 541−545.
(42) Lin, H.; Wray, L. A.; Xia, Y.; Xu, S.; Jia, S.; Cava, R. J.; Bansil, A.; Hasan, M. Z. *Nat. Mater.* **2010**, *9* (7), 546−549.
(43) Mehta, R. J.; Zhang, Y.; Karthik, C.; Singh, B.; Siegel, R. W.; Borca-Tasciuc, T.; Ramanath, G. *Nat. Mater.* **2012**, *11* (3), 233−240.
(44) Zhang, Y.; Wang, H.; Kräemer, S.; Shi, Y.; Zhang, F.; Snedaker, M.; Ding, K.; Moskovits, M.; Snyder, G. J.; Stucky, G. D. *ACS Nano* **2011**, *5* (4), 3158−3165.
(45) Xiu, F.; He, L.; Wang, Y.; Cheng, L.; Chang, L.-T.; Lang, M.; Huang, G.; Kou, X.; Zhou, Y.; Jiang, X.; Chen, Z.; Zou, J.; Shailos, A.; Wang, K. L. *Nat. Nanotechnol.* **2011**, *6* (4), 216−221.
(46) Ithurria, S.; Tessier, M. D.; Mahler, B.; Lobo, R. P. S. M.; Dubertret, B.; Efros, A. L. *Nat. Mater.* **2012**, *10* (12), 936−941.
(47) Kim, Y. S.; Brahlek, M.; Bansal, N.; Edrey, E.; Kapilevich, G. A.; Iida, K.; Tanimura, M.; Horibe, Y.; Cheong, S.-W.; Oh, S. *Phys. Rev. B* **2011**, *84* (7), 073109.
(48) Liu, C.-X.; Zhang, H.; Yan, B.; Qi, X.-L.; Frauenheim, T.; Dai, X.; Fang, Z.; Zhang, S.-C. *Phys. Rev. B* **2010**, *81* (4), 041307.
(49) Cho, S.; Butch, N. P.; Paglione, J.; Fuhrer, M. S. *Nano Lett.* **2011**, *11* (5), 1925−1927.
(50) Novoselov, K. S.; Geim, A. K.; Morozov, S. V.; Jiang, D.; Zhang, Y.; Dubonos, S. V.; Grigorieva, I. V.; Firsov, A. A. *Science* **2004**, *306* (5696), 666−669.